3D Multispectral Light Propagation Model For Subcutaneous Veins Imaging

Vincent Paquit[a,b], Jeffery R. Price[a], Fabrice Mériaudeau[b] and Kenneth W. Tobin[a]

[a] Oak Ridge National Laboratory, P.O. Box 2008, Oak Ridge, TN 37831, USA;
[b] Le2i, University of Burgundy, 12 rue de la Fonderie, 71200 Le Creusot, FRANCE

ABSTRACT

In this paper, we describe a new 3D light propagation model aimed at understanding the effects of various physiological properties on subcutaneous vein imaging. In particular, we build upon the well known MCML (Monte Carlo Multi Layer) code and present a tissue model that improves upon the current state-of-the-art by: incorporating physiological variation, such as melanin concentration, fat content, and layer thickness; including veins of varying depth and diameter; using curved surfaces from real arm shapes; and modeling the vessel wall interface. We describe our model, present results from the Monte Carlo modeling, and compare these results with those obtained with other Monte Carlo methods.

Keywords: OPT, SCAT, SIM

1. INTRODUCTION

There are an estimated one billion venipunctures and 250 million intravenous (IV) catheterizations performed annually in the United States [1]. Furthermore, approximately 20% of the venipunctures require three attempts on average while 10% of IV administrations result in some degree of extravasation, or leakage of the drug into the tissues around the injection site. Repeated attempts cause unnecessary pain and anxiety while the consequences of extravasation can range from mild, such as skin redness, to extreme, such as tissue necrosis. It is with these facts in mind that we pursue improvements in visualizing subcutaneous veins.

In earlier work [2], we noted variations in venous image quality and contrast related to both wavelength and physiological parameters, such as skin tone and/or body fat. We observed that NIR imaging might be effective or ineffective, dependent on physiological parameters. Though such variations might be expected considering existing models and studies on light propagation in tissues [3,4] with respect to subcutaneous venous imaging. Furthermore, in exploring the literature related to photon transport modeling as it relates to venous imaging, we observed that the following factors are poorly addressed: (1) the effects of physiological variation such as skin tone/melanin concentration, hydration, fat content, and/or skin thickness; (2) the vessel wall interfaces; (3) the effects of arm surface curvature and (4) the combined effects of vein depth and diameter.

In this paper, we propose a new model combining some of the existing Monte Carlo methods in order to improve light propagation modeling efficiency and we address some of the issues of these models. We present a multi-layer skin model based upon the current research and include veins. We model the vessel wall itself, estimating the multispectral optical properties from the literature [5] and through molecular comparison with similar tissues through histological literature review. We employ non-planar surfaces based on the shapes of the real arms acquired via structured light imaging developed in our previous work. We investigate changes in light propagation (image characteristics) based on changes in eight physiological parameters: (1) vein depth, (2) vein diameter, (3) tissue layer thicknesses, (4) melanin concentration, (5) water concentration, (6) blood concentration, (7) blood oxygenation, and (8) fat content.

The paper is organized as follows. Section 2 presents an overview of the current state of the art. In Section 3, we justify our choices and present our methodology, then we present some preliminary results in section 3.5. Section 4 concludes the paper and highlights future work.

Further author information: (Send correspondence to V.P.)
V.P. : E-mail: paquitvc@ornl.gov, Telephone: 1 865 241 3302

†This paper was prepared by the OAK RIDGE NATIONAL LABORATORY, Oak Ridge, Tennessee, 37831-6285, operated by UT-BATTELLE, LLC for the U.S. DEPARTMENT OF ENERGY under contract DE-AC05-00OR22725.

Medical Imaging 2008: Physics of Medical Imaging, edited by Jiang Hsieh, Ehsan Samei,
Proc. of SPIE Vol. 6913, 69130D, (2008) · 1605-7422/08/$18 · doi: 10.1117/12.772825

2. STATE OF THE ART

Modeling the color appearance of the skin under different illuminants has been investigated for biomedical applications in order to diagnose skin disorders based on spectral reflectance analysis [6] and to characterize skin structure. Several mathematical models have been implemented and the majority of them are based on two main techniques: the Kubelka-Munk light transport method, giving accurate reflectance and transmittance profiles of multi-layered turbid medium with a short computation time, and the Monte Carlo light propagation models, giving very accurate reflectance and transmittance profiles but with a significantly longer computation time. Monte Carlo models are considered very accurate and are used as references for the comparison of algorithms. Therefore we initially built our model on this method first. An implementation of our model using the Kubelka-Munk theory will be investigated in future research.

In this section we will discuss only the most interesting approaches, analyzing the propagation of photons in skin tissues using the Monte Carlo simulation and identifying the improvements required in order to achieve our goal. Monte Carlo simulations are commonly used to analyze light propagation in biological tissues. In these simulations, each model considers the same statistical approaches of the interaction process between photons and tissue layers, detailed in [7]. However methodologies differ due to individual interpretation of the skin structure and experimental requirements.

Jacques et al. [4, 7, 8] developed a well known model publicly available online called MCML. This model takes into account the presence of multiple layers in the skin. The authors consider the skin as a succession of layers and vessels infinitely wide and assume the photon beam direction as perpendicular to the surface of the skin. They define a cylindrical referential by radial revolution around the beam axis in order to easily record the energy distribution of all propagation events in up to two dimensions arrays instead of in a volume. However if these hypothesis correctly model small skin volumes, they are not valid if we lose the symmetrical revolution property i.e. if the width of the light beam is greater than the size of a structure that may be observed. For this reason, it is not suitable to simulate reflectance images of a large area.

Meglinski et al. [9] introduced a more realistic model considering a higher subdivision of the skin into layers based on their molecular characteristics. This allows for the computation of the absorption coefficients in each layer, based on both the molar fraction of particles present and the wavelength. In addition, the model includes a periodic parameterization of the layer transitions, pointing out the necessity for realistic 3D modeling of the skin. However in this model a vessel is considered as infinitely wide, and furthermore the model does not include the curvature information of the surface.

Nishidate et al. [10] introduced a model to locate and measure subcutaneous veins by the analysis of diffuse reflectance images over a large skin area at different wavelengths. While the theoretical and experimental protocol for tissue phantoms sounds promising, their approach seems to be incomplete for the case of real subjects. This is for three main reasons: 1) the curvature of the surface of the skin has to be known in order to accurately calculate the incident angle of each photon entering the skin, and also to calculate the quantity of energy left after specular reflection on the surface; 2) the non-radial symmetry of the system is not considered leading to errors in reflectance, absorption and transmittance calculations; 3) they do not consider the possibility that a photon leaving the skin cannot be seen by the camera due to its direction vector. These three issues may explain why the authors report large measurement errors in the case of an in-vivo experiment (error: depth 30%, thickness 19%).

3. METHODS

In this paper we present a method which includes computational models of the subcutaneous tissue and veins. We simulate photon transport and imaging using Monte Carlo modeling. We began with routines in the publicly available MCML (Monte Carlo Multi-Layer) code [7] and made several significant modifications to the code to achieve more realistic modeling of the tissue, accurate simulation of imaging and code optimization. In particular, we have integrated the following contributions to the state-of-the art:

- We construct a complex multi-layer skin model based upon the current research [7,9,11,12] and also include veins.
- We allow changes in light propagation (image characteristics) based on changes in 8 parameters: (1) vein depth, (2) vein diameter, (3) tissue layer thicknesses, (4) melanin concentration, (5) water concentration, (6)

blood concentration, (7) blood oxygenation, and (8) fat content. Standard ranges for these parameters will be gathered from a survey of histological literature.
Light propagation models based on Monte Carlo simulation, use the same statistical approaches to characterize the different interaction events between photons and the medium. We use the same strategy and we advise the reader to access the original document from Prahl et al. [4] where all the statistical equations are well defined and documented. Based on our remarks section 2, we made the hypothesis that creating a more realistic 3D model of the skin structure will lead to a better approximation of light propagation in turbid medium. In this section, we define the characteristics of our light propagation model and explain how we address some of the issues mentioned previously.

3.1. Skin structure and optical properties

The skin is the largest organ of our body. Anatomically, it is characterized by a succession of three principal layers (from top to bottom):
- the epidermis contains a large fraction of the chromophores of the skin defining the overall skin tone;
- the dermis contains blood vessels, nerves and structural molecules;
- the hypodermis, also called subcutaneous tissue, is the lowest layer below the skin. It contains large blood vessels, fat and connective tissues. Notice, it is physiologically not considered as a layer of the skin. However, since the subcutaneous vessel that we want to localize are embedded in the hypodermis, we must integrate this layer to our skin model.

Each sublayer presenting established molecular particularities, Meglinski et al. [9] created a model with seven layers to accurately simulate the propagation of photons at a microscopic scale. However, if their study requires modeling the skin with such a precision, we can reduce the number of layers to the three previously cited since large reflectance variations are not expected when imaging a large skin area. In addition, Monte Carlo simulation are expensive computation wise and reducing the number of layers will decrease the complexity of the photon propagation process and furthermore the computation time.
In Monte Carlo models, the photon propagation is characterized by the interaction process with the molecules present in the medium, and also by the collision at the transition between layers detailed in section 3.2. There are two types of molecular interaction: scattering and absorption, both defined respectively by scattering coefficients and absorption coefficients. Past studies in the field have characterized these coefficients over the electromagnetic spectrum and for a large number of molecules contained in the different sublayers of the skin. We consider the review made by Jacques et al. [13] as the main source of data for this study. In the following we list for each element of our model the anisotropy factor $g(\lambda)$, the refractive index n, the scattering coefficient $\mu_s(\lambda)$ and absorption coefficient $\mu_a(\lambda)$. Since the optical properties of the vessel wall and the subcutaneous layer are not well documented, we have made the following assumption: (1) the structure of blood vessel is assimilated to the structure of the aorta for which the optical properties are listed in [5], (2) since we can assimilate the blood vessels as an entity in our model, the hypodermis is approximated as a layer containing fat and connective tissues. We also limit the influence of blood to define the optical properties of the hypodermis.

3.1.1. Anisotropy factor

The anisotropy factor is the average cosine of the scattering angle. At a given wavelength it corresponds to the probable deflection angle resulting of a scattering event. In [14], Gemert et al. define the anisotropic factor for dermis and epidermis as a function of wavelength:

$$g_{Dermis} = g_{Epidermis} = 0.62 + 0.29 \times \lambda \times 10^{-3} \quad (1)$$

According to Roggan et al. [15], the blood anisotropic factor is approximately constant over the range 450nm - 1100 nm and can be averaged as: $g_{Blood} = 0.99$. The blood vessel anisotropic factor is $g_{Vein} = 0.9$ [5] and the fat anisotropic factor is $g_{Hypodermis} = 0.75$ [9].

3.1.2. Scattering coefficients

In biological tissues, the scattering effect corresponds to the phenomenon in which the direction of a wave changes after interaction with an element in the medium. The scattering influence of this element is quantified

by the scattering coefficient as a function of wavelength. In [13], the reduced scattering properties of dermis $\mu_{s,Dermis}^{'}(\lambda)$ and epidermis $\mu_{s,Epidermis}^{'}(\lambda)$ are considered equal and are presented as the combination of the interaction with large molecules (Mie scattering) and with small molecules (Rayleigh scattering), respectively $\mu_{s,Mie}(\lambda)$ and $\mu_{s,Mie}(\lambda)$ in the following equations:

$$\mu_{s,Mie}(\lambda) = (2 \times 10^5) \times \lambda^{-1.5} \qquad [cm^{-1}] \tag{2}$$

$$\mu_{s,Rayleigh}(\lambda) = (2 \times 10^{12}) \times \lambda^{-4} \qquad [cm^{-1}] \tag{3}$$

$$\mu_{s,Dermis}^{'}(\lambda) = \mu_{s,Epidermis}^{'}(\lambda) = \frac{\mu_{s,Rayleigh}(\lambda) + \mu_{s,Mie}(\lambda)}{1 - g(\lambda)} \qquad [cm^{-1}] \tag{4}$$

The reduced scattering coefficients for veins $\mu_{s,Vein}^{'}$ and blood $\mu_{s,Blood}^{'}$ were respectively derived from Oraevsky et al. [5] and from Roggan et al. [15]. The reduced scattering coefficients for the hypodermis $\mu_{s,Hypodermis}^{'}$ is defined by [16]:

$$\mu_{s,Hypodermis}^{'} = 1050.6 \times \lambda^{-0.68} \qquad [cm^{-1}] \tag{5}$$

Figure 1 plots the scattering coefficients over wavelength used in our Monte Carlo simulation.

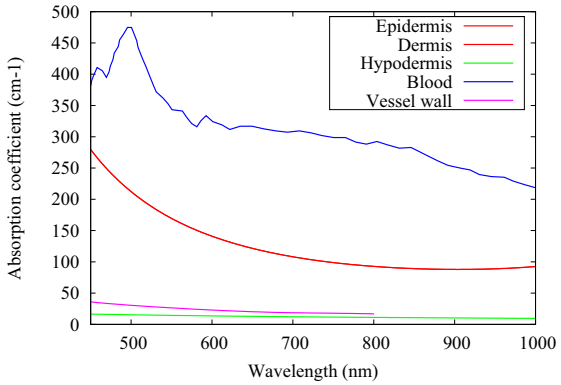

Figure 1. Scattering coefficients of the skin layers considered in our Monte Carlo simulation.

3.1.3. Absorption coefficients

The absorption event corresponds to the attenuation of photon energy due to absorption by a particle or group of particles. With each skin layer being composed of several molecules, the absorption coefficient of a layer is a function of the molar concentration and the absorption coefficient of the molecules present. The absorption coefficient of a layer is given by the following equation [9]:

$$\mu_a(\lambda) = \sum_{i=1}^{m} \left(\mu_a^{(i)}(\lambda) C_i \prod_{j=1}^{i-1} (1 - C_j) \right) + \mu_a^{(0)}(\lambda) \prod_{i=1}^{m} (1 - C_i). \tag{6}$$

where C_i is the volume fraction of the ith molecule, m is the total number of molecules contained in the layer, $\mu_a^{(i)}(\lambda)$ is the absorption coefficient of the ith absorber, $\mu_a^{(0)}(\lambda)$ is the absorption coefficient of the medium free of any absorbers. Figure 2(a) plots, over wavelength, the absorption coefficients of oxy-hemoglobin $\mu_a^{HbO2}(\lambda)$ and desoxy-hemoglobin $\mu_a^{Hb}(\lambda)$ [17], water $\mu_a^{H_2O}(\lambda)$ [18], melanin $\mu_a^{Melanine}(\lambda)$ (equation 7) and for the medium free of absorbers $\mu_a^0(\lambda)$ (equation 8).

$$\mu_a^{Mel}(\lambda) = 6.6 \times 10^{11} \times \lambda^{-3.33} \qquad [cm^{-1}] \tag{7}$$

$$\mu_a^0(\lambda) = 7.84 \times 10^8 \times \lambda^{-3.255} \qquad [cm^{-1}] \tag{8}$$

Figure 2(b) plots, over wavelength, the absorption coefficients of the layers considered in our model based on the equations given by Meglinski et al. [9] and with the parameters listed table 2(b). C_{blood} and C_{H_2O} are respectively the volume fraction of blood and water in each layers and n the refractive index. Despite the conclusion of Schmitt et al. [19] we define constant values of the refractive index for the entire range of study based on average values from the literature. The listed values represent the average molar fraction of a Caucasian individual and should not be considered as representative of the entire population. In addition, keep in mind that these parameters vary in different parts of the body.

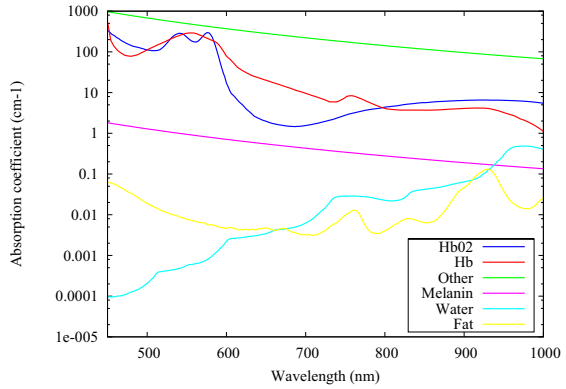

(a)

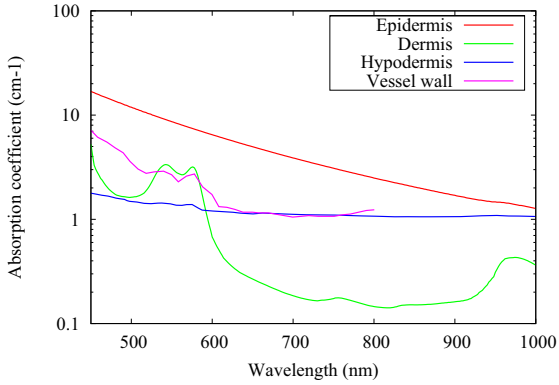

(b)

	C_{Blood}	C_{H_2O}	C_{Fat}	C_{Mel}	$n(\lambda)$
Epidermis	0.0	0.2	0.0	0.02	1.34
Dermis	0.12	0.65	0.0	0.0	1.4
Vessel wall	-	-	-	-	0.98
Blood	-	-	-	-	0.98
Hypodermis	0.05	0.7	0.56	0.0	1.44

(c)

Figure 2. (a) Absorption coefficients of the molecules in presence, (b) Absorption coefficients of each layer, (c) Molar fraction of each absorber. It is important to note that C_{H_2O}, C_{Fat} and C_{Mel} represent the fractions after the blood volume has been subtracted from the tissue. We do not list concentration values for vessel wall and blood since we use measured data.

3.2. Modeling the layers

When a photon is propagating through the interface between two layers, the remaining energy of this photon will be either reflected or transmitted in a new direction, changing significantly the propagation process. It is then important to locate precisely the intersection point. In our model, we consider layer transitions and vein envelops as complex 3D structures represented by high dimensional parametric surfaces. Keeping in mind that in a light propagation model, for one million photons launched in the medium, there are on average 100 million photon movements, the number of collision tests with the parametric surfaces can be considerable and of course time consuming. In order to avoid solving high dimensional equations, we have opted for a geometrical approach using Bézier patches for the 3D modeling and a ray tracing intersection method called Bézier clipping. This approach presents the advantage of being both accurate and computationally fast.

3.2.1. Bézier surface

Bézier surfaces were introduced by Pierre Bézier in 1972 [20] to design automobile bodies with a simplified modeling method. By analogy, the surface of the skin can be modelled as an element of an automobile body: globally smooth, curved and presenting a real change in shape at the junctions. We parameterize the 3D surface of the skin with a $(m \times n)$ dimensional Bézier patch defined by a set of $(m+1) \times (n+1)$ control points $C_{i,j}$. Each

point P on the surface being approximated over the unit square as a function of two parametric coordinates u and v by the following equation:

$$P(u,v) = \sum_{i=0}^{m} B_i^m(u) \left[\sum_{j=0}^{n} B_j^n(v)\, C_{i,j} \right] \tag{9}$$

with $B_i^m(u)$ and $B_j^n(v)$ Bernstein polynomials defined by:

$$B_a^b(c) = \frac{b!}{a!(b-a)!}\, c^a (1-c)^{b-a} \tag{10}$$

Equation 9 is in fact a tensor product and can be written as a product of matrices as follow:

$$\mathbf{P}(u,v) = \mathbf{M}_{B_i^m}(u) \times \mathbf{M}_{C_{i,j}} \times \mathbf{M}_{B_j^n}^T(v) \tag{11}$$

Figure 3(a) shows a grid of control points (yellow) parameterizing the Bézier surface (white).

3.2.2. Bézier clipping

In 1990, Nishita et al. [21] described an iterative algorithm called Bézier clipping to compute intersections between a ray and a Bézier patch. By identifying and cutting away regions of the patch that are not intersecting the ray, the algorithm converge by dichotomy to a list of all acceptable intersection points for a given initial precision value ε. We use Efremov et al. [22] implementation since they improved the initial algorithm and also address stability issues. For each intersection point, we compute the normal on the Bézier surface to calculate the incident angle of the photon path. Figure 3(b) is an example of collision detection by Bézier clipping.

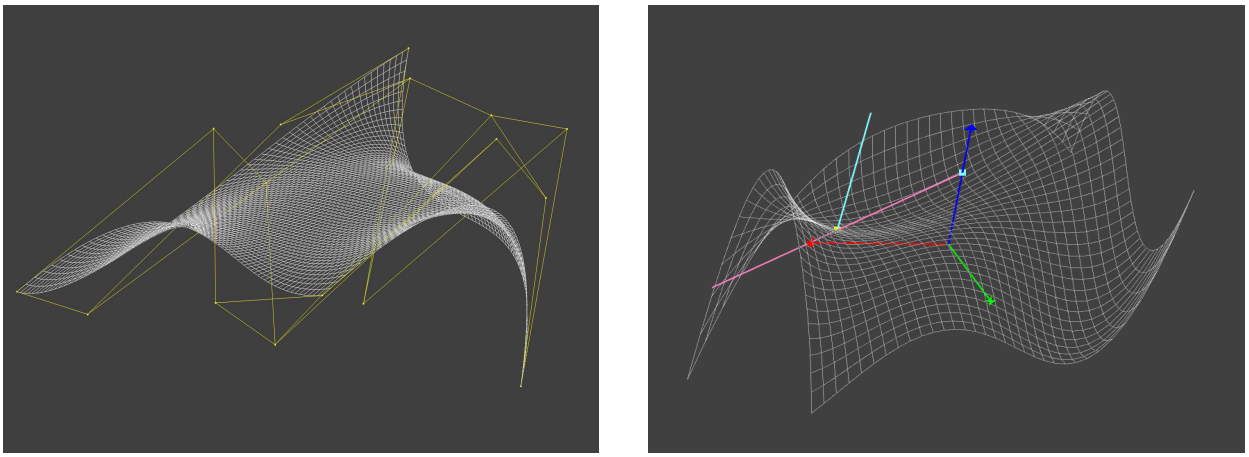

(a) (b)

Figure 3. (a) Bézier surface (white) with its grid of control points (yellow), (b) Example of intersection detection where the purple line correspond to the ray intersecting the surface. The resulting normal is drawn in cyan.

3.3. Experimental setup

Previous research [3] has investigated the propagation of light in tissue as a function of wavelength, showing a higher penetration of near-infrared (NIR) light into the tissue and a lower sensitivity to the pigmentation of the skin. Our experimental setup has been designed to exploit these interesting characteristics with the aim of evaluating the depth of subcutaneous structures and also to extend our model to a large range of skin tone. Our acquisition system (Figure 4) is composed of a NIR sensitive CMOS camera with a 740nm long-pass

interferometric filter, a NIR illumination source, a NIR line-generating laser module and a diffuser in front of the light source for illumination homogeneity. Once all the components of the acquisition benchtop are fixed in an optimal configuration, the system is calibrated in two consecutive phases for image distortion correction using the method described in [23] and the 3D reconstruction parameterization.

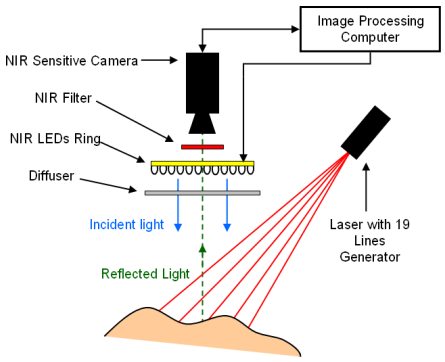

Figure 4. Acquisition setup

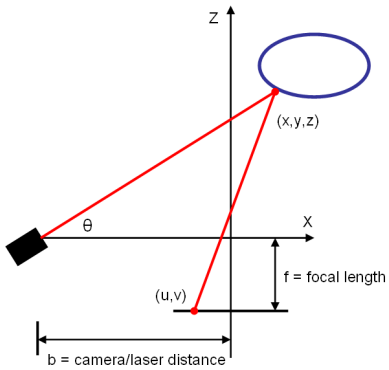

Figure 5. Triangulation principle

3.4. 3D reconstruction process

We generate the 3D model of the skin used in our Monte Carlo simulation from a real 3D skin surface measurement and the sub-layers are computed as homotheties of the surface mesh to maintain a uniform thickness. The 3D reconstruction process of the surface of the skin uses active optical triangulation by combining a camera and a laser stripe line generator [24]. The geometry of the laser triangulation is shown in Figure (5). The camera is aligned along the Z axis and the laser line generator is positioned at a distance b from the camera with the angle θ relative to the X axis. Assuming that the considered laser point coordinates (x, y, z) in the 3D baseline has a projection (u, v) on the image plane, the similar triangles equations give the mathematical relation between the measured quantities (u, v, θ) and the coordinates (x, y, z):

$$[x, y, z] = \frac{b}{f.\cot\theta - u}[u, v, f]. \tag{12}$$

Parameters b, f and θ are calculated during the system calibration and remain constant during the acquisition phase. In a NIR image of the laser lines on the surface of the skin (figure 6.a), the centerline of each line is firstly detected using a curvilinear structures detector [25] (figure 6.b) and secondly triangulated using equation (12) (figure 6.c). The resulting point cloud is then approximated by a Bézier patch using equation (11), as shown Figure 6.e. In this case, $\mathbf{P}(u, v)$ is the matrix of the triangulated points, and $\mathbf{M}_{B_i^m(u)}$ and $\mathbf{M}_{B_j^n(v)}$ are calculated from equation (10). The matrix $\mathbf{M}_{C_{i,j}}$ corresponding to the Bézier control points is then calculated from (11):

$$\mathbf{M}_{C_{i,j}} = \mathbf{M}_{B_i^m}^{-1}(u) \times \mathbf{P}(u, v) \times \mathbf{M}_{B_j^n}^{-T}(v) \tag{13}$$

The dimensions m and n of the control point matrix are recursively evaluated by fitting error minimization with a precision value ε arbitrary defined. In a last step, Figure 6.f, each transition layer is created as a homothety of the external layer and added to the model in order to build the complex 3D skin volume. The position of one or more blood vessel is evaluated from the NIR images and is positioned in the 3D volume as a perfect cylinder. We are currently investigating methods to automate the procedure and to dynamically model the subcutaneous vessel from reflectance images of the skin surface.

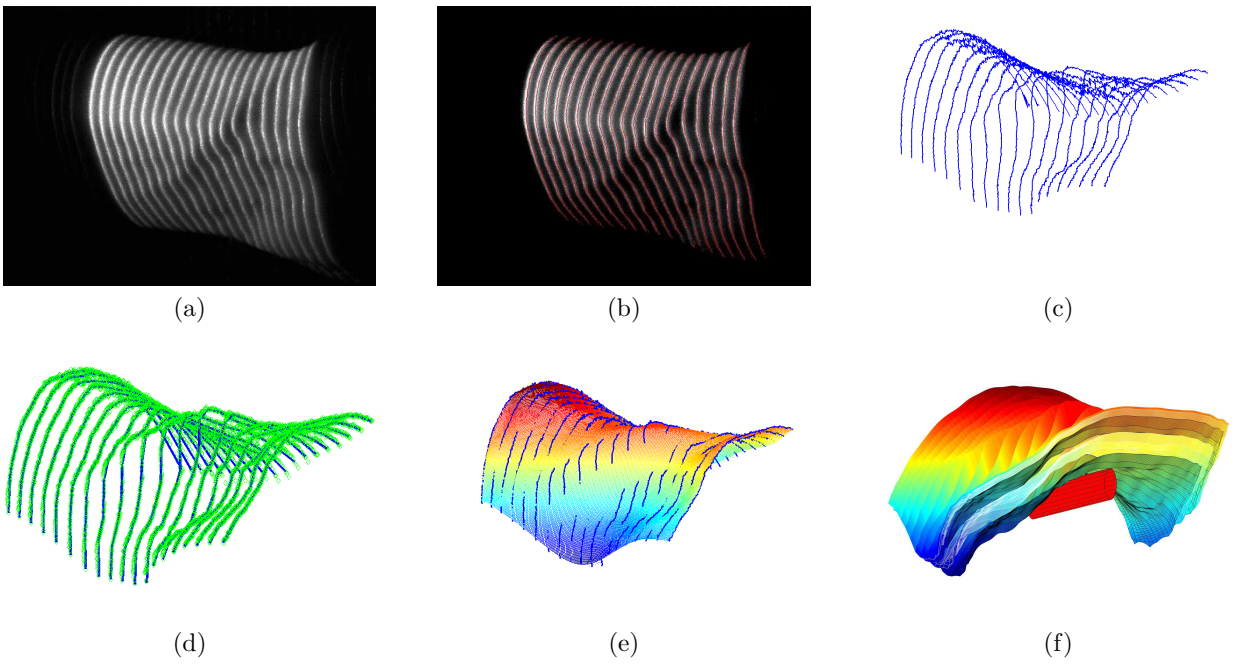

Figure 6. (a) NIR image of the laser lines, (b) Centerline detection, (c) Result of the centerline triangulation into a 3D point cloud, (d) Approximation of the 3D point cloud (green) with Bézier curves (blue), (e) Approximation of the 3D point cloud with a Bézier patch, (f) 3D model of a complex skin structure including one vein.

3.5. Comparative results

To validate our model we first compare diffuse reflectance and absorption results from our model to MCML corresponding results. In order to compare both models we defined, as stated previously, a three layer model of the skin including vein with the parameters listed in table Figure 7 where μ_s is the scattering coefficient, μ_a the absorption coefficient, g the anisotropy factor, n the refractive index, d is the thicknesses of the layers. Each layer is considered infinitely wide and parallel. Figure 7.a presents comparative results of the diffuse reflectance and Figure 7.b presents comparative results of the absorption as a function of the depth. We can see that both techniques match perfectly. We firstly conclude that our complex 3D modeling and collision detection methods do not alter the results of the MCML simulation.
As a second experiment we compare the absorption results simulated with both Monte Carlo methods in order to determine which model characterizes realistic light propagation in a complex 3D volume. We initialize both models with the parameters listed in the table Figure 8. The MCML model includes infinite parallel layers and veins. Our model includes infinite parallel layers and one cylindrical vein. We choose this configuration in order to compare both models closely. As one can see Figure 8.a and Figure 8.b, the energy absorption in the medium is significantly different and appears to be influenced by the shape of the subcutaneous vessel. This lets us assume that our method is more accurate regarding photon collision events in the medium and gives a better characterization of light propagation in biological tissues.

4. CONCLUSION

In this paper we have presented a new tissue model and Monte Carlo approach to better understand the effects of varying anatomical parameters on the propagation of light in biological tissues. We have presented a more realistic 3D light propagation model, and discussed its effectiveness by comparing simulated reflectance and absorption results of a skin area containing subcutaneous vein with simulation results of a well known existing model.

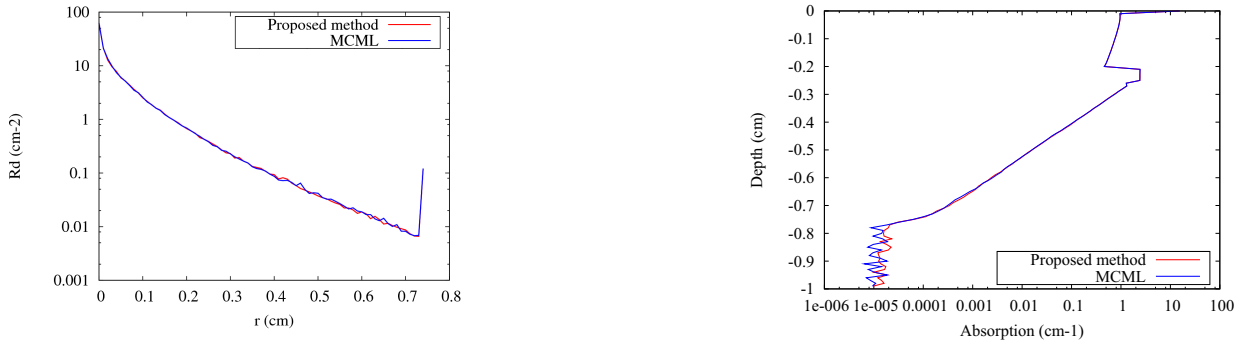

(a) (b)

$\lambda = 700nm$	C_{Blood}	C_{H_2O}	C_{Fat}	C_{Mel}	$n(\lambda)$	$\mu_s(\lambda)$ (cm^{-1})	$\mu_a(\lambda)$ (cm^{-1})	$g(\lambda)$ (-)	d (cm)
Epidermis	0.0	0.2	0.0	0.02	1.34	108.07	3.88	0.765	0.01
Dermis	0.12	0.65	0.0	0.0	1.4	108.07	0.21	0.765	0.2
Hypodermis	0.05	0.7	0.56	0.0	1.44	12.21	1.36	0.75	0.05
Vessel wall	-	-	-	-	0.98	18.61	1.05	0.9	0.005
Blood vessel	-	-	-	-	0.98	308.23	1.55	0.98	0.5
Vessel wall	-	-	-	-	0.98	18.61	1.05	0.9	0.005
Hypodermis	0.05	0.7	0.56	0.0	1.44	12.21	1.36	0.75	0.23

Figure 7. Comparative results between our model and MCML: (a) diffuse reflectance, (b) absorption

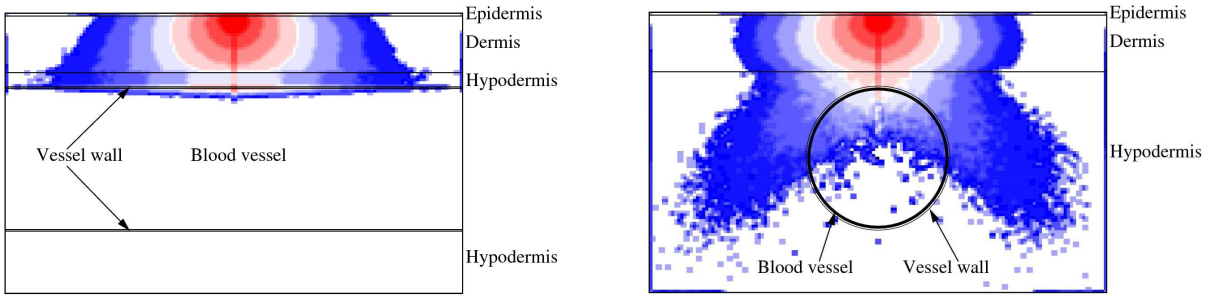

(a) (b)

$\lambda = 500nm$	C_{Blood}	C_{H_2O}	C_{Fat}	C_{Mel}	$n(\lambda)$	$\mu_s(\lambda)$ (cm^{-1})	$\mu_a(\lambda)$ (cm^{-1})	$g(\lambda)$ (-)	d (cm)
Epidermis	0.0	0.2	0.0	0.02	1.34	219.29	11.87	0.765	0.01
Dermis	0.12	0.65	0.0	0.0	1.4	212.29	1.94	0.765	0.2
Hypodermis	0.05	0.7	0.56	0.0	1.44	15.35	1.06	0.75	0.05
Vessel wall	-	-	-	-	0.98	30.51	3.50	0.9	0.005
Blood vessel	-	-	-	-	0.98	474.75	112.11	0.99	0.5
Vessel wall	-	-	-	-	0.98	30.51	3.50	0.9	0.005
Hypodermis	0.05	0.7	0.56	0.0	1.44	15.35	1.06	0.75	0.23

Figure 8. Comparative results between our model and MCML: (a) absorption of photon energy in the case of a 3D model where all layers are flat, (b) absorption of photon energy with our model, considering a more complex 3D skin structure

REFERENCES

1. H. Ogden-Grable and G. W. Gill, "Phlebotomy puncture juncture: Preventing phlebotomy errors–potential for harming your patients," *Laboratory Medicine* **36**(7), pp. 430–433, 2005.
2. V. Paquit, J. R. Price, F. Meriaudeau, J. Kenneth W. Tobin, and T. L. Ferrell, "Combining near-infrared illuminants to optimize venous imaging," *Medical Imaging 2007: Visualization and Image-Guided Procedures* **6509**(1), p. 65090H, SPIE, 2007.
3. T. Vo-Dinh, *Biomedical Photonics Handbook*, CRC Press, Boca Raton, 2003.

4. S. A. Prahl, M. Keijzer, S. L. Jacques, and A. J. Welch, "A Monte Carlo model of light propagation in tissue," in *SPIE Proceedings of Dosimetry of Laser Radiation in Medicine and Biology*, G. J. Müller and D. H. Sliney, eds., **IS 5**, pp. 102–111, 1989. monte carlo.
5. S. L. Jacques, "Optical properties of aorta," 1998. http://omlc.ogi.edu/spectra/aorta/index.html.
6. S. Cotton and E. Claridge, "Developing a predictive model of human skin coloring," *Medical Imaging 1996: Physics of Medical Imaging* **2708**(1), pp. 814–825, SPIE, 1996.
7. W. Lihong, S. Jacques, and Z. Liqiong, "MCML - monte carlo modeling of light transport in multi-layered tissues," *Computer Methods and Programs in Biomedicine* **47**, pp. 131–146(16), July 1995.
8. S. L. Jacques, I. S. Saidi, and F. K. Tittel, "Average depth of blood vessels in skin and lesions deduced by optical fiber spectroscopy," in *Proc. SPIE Vol. 2128, p. 231-237, Laser Surgery: Advanced Characterization, Therapeutics, and Systems IV, R. Rox Anderson; Ed.*, R. R. Anderson, ed., *Presented at the Society of Photo-Optical Instrumentation Engineers (SPIE) Conference* **2128**, pp. 231–237, Sept. 1994.
9. I. V. Meglinski and S. J. Matcher, "Quantitative assessment of skin layers absorption and skin reflectance spectra simulation in the visible and near-infrared spectral regions," *Physiological Measurement* **23**(4), pp. 741–753, 2002.
10. I. Nishidate, T. Maeda, Y. Aizu, and K. Niizeki, "Visualizing depth and thickness of a local blood region in skin tissue using diffuse reflectance images.," *J Biomed Opt* **12**(5), p. 054006, 2007.
11. L. F. Douven and G. W. Lucassen, "Retrieval of optical properties of skin from measurement and modeling the diffuse reflectance," in *Proc. SPIE Vol. 3914, p. 312-323, Laser-Tissue Interaction XI: Photochemical, Photothermal, and Photomechanical, Donald D. Duncan; Jeffrey O. Hollinger; Steven L. Jacques; Eds.*, D. D. Duncan, J. O. Hollinger, and S. L. Jacques, eds., *Presented at the Society of Photo-Optical Instrumentation Engineers (SPIE) Conference* **3914**, pp. 312–323, June 2000.
12. W. F. Cheong, S. A. Prahl, and A. J. Welch, "A review of the optical properties of biological tissues," *IEEE J. Quantum Electron.* **26**, pp. 2166–2185, 1990.
13. S. L. Jacques, "Skin optics," 1998. http://omlc.ogi.edu/news/jan98/skinoptics.html.
14. M. Van Gemert, S. Jacques, H. Sterenborg, and W. Star, "Skin optics," *Biomedical Engineering, IEEE Transactions on* **36**(12), pp. 1146–1154, Dec 1989.
15. A. Roggan, M. Friebel, K. Dorschel, A. Hahn, and G. Muller, "Optical properties of circulating human blood in the wavelength range 400–2500 nm," *Journal of Biomedical Optics* **4**(1), pp. 36–46, 1999.
16. V. I. K. A N Bashkatov, E A Genina and V. V. Tuchin, "Optical properties of human skin, subcutaneous and mucous tissues in the wavelength range from 400 to 2000nm," *Journal of Physics D: Applied Physics* **38**(15), pp. 2543–2555, 2005.
17. S. A. Prahl, "Optical absorption of hemoglobin," 1998. http://omlc.ogi.edu/spectra/hemoglobin.
18. G. M. Hale and M. R. Querry, "Optical constants of water in the 200-nm to 200-micrometer wavelength region," *Appl. Opt.* **12**(3), p. 555, 1973.
19. J. M. Schmitt and G. Kumar, "Turbulent nature of refractive-index variations in biological tissue," *Optics Letters* **21**, pp. 1310–1312, Aug. 1996.
20. P. E. Bezier, *Emploi des machines a commande numerique*, Masson et Cie., 1970. Translated by Forrest, A. Robin and Pankhurst, Anne F. as Numerical Control – Mathematics and Applications, John Wiley and Sons, Ltd., London, 1972.
21. T. Nishita, T. W. Sederberg, and M. Kakimoto, "Ray tracing trimmed rational surface patches," *SIGGRAPH Comput. Graph.* **24**(4), pp. 337–345, 1990.
22. A. Efremov, V. Havran, and H.-P. Seidel, "Robust and numerically stable bezier clipping method for ray tracing nurbs surfaces," in *SCCG 2005*, pp. 123–131, ACM, 2005.
23. Z. Zhang, "Flexible Camera Calibration by Viewing a Plane from Unknown Orientations," in *ICCV*, pp. 666–673, 1999.
24. P. J. Besl, *Surfaces in range image understanding*, Springer-Verlag New York, Inc., New York, NY, USA, 1988.
25. C. Steger, "Extraction of curved lines from images," in *13th International Conference on Pattern Recognition*, **2**, pp. 251–255, 1996.